

---

# Climate Data Record (CDR) Program

## Climate Algorithm Theoretical Basis Document (C-ATBD)

### AVHRR Polar Pathfinder (APP)



CDR Program Document Number: CDRP-ATBD-0572  
Revision 2 / February 07, 2019

**REVISION HISTORY**

<b>Rev.</b>	<b>Author</b>	<b>DSR No.</b>	<b>Description</b>	<b>Date</b>
1	Yinghui Liu, CIMSS UW-Madison; Jeff Key, NOAA; Andrew Heidinger, NOAA	DSR-734	Initial baseline submission to the CDR Program Library	09/16/2015
2	Yinghui Liu, Jeff Key, Xuanji Wang	DSR-1334	Final update for APP v2.0	02/07/2019

## TABLE of CONTENTS

<b>1. INTRODUCTION.....</b>	<b>6</b>
1.1 Purpose.....	6
1.2 Definitions.....	6
1.3 Document Maintenance.....	7
1.4 Improvements in APP v2.0 .....	7
<b>2. OBSERVING SYSTEMS OVERVIEW.....</b>	<b>8</b>
2.1 Products Generated .....	8
2.2 Instrument Characteristics .....	8
<b>3. ALGORITHM DESCRIPTION.....</b>	<b>12</b>
3.1 Algorithm Overview .....	12
3.2 Processing Outline.....	12
3.2.1 Data Ingest .....	14
3.2.2 Calibration.....	14
3.2.3 Navigation.....	14
3.2.4 Compositing .....	14
3.3 Algorithm Input.....	15
3.3.1 Primary Sensor Data .....	15
3.3.2 Ancillary Data.....	15
3.3.3 Derived Data .....	16
3.3.4 Forward Models.....	16
3.4 Theoretical Description .....	16
3.4.1 Physical and Mathematical Description.....	16
3.4.2 Data Merging Strategy.....	19
3.4.3 Numerical Strategy .....	19
3.4.4 Calculations.....	19
3.4.5 Look-Up Table Description.....	20
3.4.6 Parameterization .....	20
3.4.7 Algorithm Output.....	20
<b>4. TEST DATASETS AND OUTPUTS.....</b>	<b>21</b>
4.1 Test Input Datasets .....	21
4.2 Test Output Analysis .....	21
4.2.1 Reproducibility.....	21
4.2.2 Precision and Accuracy .....	23
4.2.3 Error Budget.....	24
<b>5. PRACTICAL CONSIDERATIONS.....</b>	<b>24</b>
5.1 Numerical Computation Considerations.....	25
5.2 Programming and Procedural Considerations .....	25
5.3 Quality Assessment and Diagnostics .....	25
5.4 Exception Handling .....	25

5.5 Algorithm Validation ..... 25

5.6 Processing Environment and Resources ..... 25

**6. ASSUMPTIONS AND LIMITATIONS ..... 25**

6.1 Algorithm Performance ..... 25

6.2 Sensor Performance ..... 31

**7. FUTURE ENHANCEMENTS..... 31**

7.1 Enhancement 1 ..... 31

**8. REFERENCES..... 32**

**APPENDIX A. ACRONYMS AND ABBREVIATIONS..... 34**

## LIST of FIGURES

Figure 1: Equatorial crossing time of NOAA POES. (Figure is from <a href="http://www.star.nesdis.noaa.gov/smcd/emb/vci/VH/vh_avhrr_ect.php">www.star.nesdis.noaa.gov/smcd/emb/vci/VH/vh_avhrr_ect.php</a> . The original ECT data are from <a href="http://www.ospo.noaa.gov/Products/ppp/navpage.html">www.ospo.noaa.gov/Products/ppp/navpage.html</a> .).....	11
Figure 2: Flow chart of processing steps to generate APP from AVHRR GAC level 1b data for a single target time. ....	13
Figure 3: APP channel 1 reflectance (%) at 1400 LST of the Arctic on July 1 of the year 1982, 1986, 1989, 1996, 2002, and 2007. ....	22
Figure 4: APP channel 4 BT (K) at 1400 LST of the Antarctic on January 1 of the year 1982, 1986, 1989, 1996, 2002, and 2007. ....	22
Figure 5: Channel 1 reflectance (%) and channel 4 BT (K) at 1400 LST of the Arctic on July 1 of the year 2007 from APP (upper row) and MODIS Aqua (lower row).....	24
Figure 6: Time series of monthly average AVHRR channel 4 brightness temperatures from January 1, 1982 to December 31, 1999 at Barrow, Alaska for 1400 local solar time. Note: there are no data available from September 14, 1994 to January 18, 1995. ....	26
Figure 7: Time series of daily AVHRR channel 4 brightness temperatures from July 1, 1984 to July 1, 1985 at Barrow, Alaska for 1400 local solar time covering the change from NOAA-7 to NOAA-9 (vertical line). .....	27
Figure 8: Time series of daily AVHRR channel 4 brightness temperatures from July 1, 1988 to July 1, 1989 at Barrow, Alaska for 1400 local solar time, covering the change from NOAA-9 to NOAA-11 (vertical line). .....	27
Figure 9: Time series of monthly average surface skin temperatures from January 1, 1982 to December 31, 1999 at Barrow, Alaska for 1400 local solar time. Note: there are no data available from September 14, 1994 to January 18, 1995.....	28
Figure 10: Time series of the AVHRR channel 2 reflectance averaged over a 275 x 275 km <sup>2</sup> area around Vostok, Antarctica from July 1, 1984 to July 1, 1985 at a local solar time of 1400, covering the transition of NOAA-7 to NOAA-9.....	29
Figure 11: Time series of the AVHRR scan angle averaged over a 275 x 275 km <sup>2</sup> area around Vostok, Antarctica from July 1, 1984 to July 1, 1985 at a local solar time of 1400, covering the transition of NOAA-7 to NOAA-9.....	29
Figure 12: Time series of the solar zenith angles averaged over a 275 x 275 km <sup>2</sup> area around Vostok, Antarctica from July 1, 1984 to July 1, 1985 at local solar time of 1400, covering the transition from NOAA-7 to NOAA-9. ....	30

Figure 13: Histogram of Channel 2 reflectance differences (left), and Channel 4 brightness temperature differences at local solar time of 1400 on July 15, 2016. .... 31

## LIST of TABLES

Table 1. Versions of the APP CDR product release, software, and the C-ATBD. ....	7
Table 2: NOAA POES series .....	9
Table 3: Spectral specifications of AVHRR/1, /2, and /3.....	10
Table 4: NOAA POES satellites used in APP. ....	11
Table 5: Calibration slope parameters for AVHRR channels 1 and 2 (Heidinger et al., 2010).....	20
Table 6: APP output .....	21
Table 7: Summary of Errors in AVHRR Ch1, Ch2, and Ch3a reflectance data set. ....	24

# 1. Introduction

## 1.1 Purpose

The purpose of this document is to describe the algorithm used to create the AVHRR Polar Pathfinder (APP) Climate Data Record (CDR) from 1982 to the present. APP uses the observations from the Advanced Very High Resolution Radiometer (AVHRR) onboard the NOAA polar orbiting satellites. APP is a fundamental climate data record (FCDR). Its purpose is to provide calibrated and navigated sensor data for the generation of higher level geophysical parameters. In particular, it is the primary input to the eXtended AVHRR Polar Pathfinder Product, APP-x. APP-x is described in a separate C-ATBD. The algorithm is defined by the computer program (code) that accompanies this document. The purpose of this document is to provide an understanding the data processing algorithm, from both a scientific perspective, and to assist a software engineer or end-user performing an evaluation of the code or the data.

## 1.2 Definitions

The following is a summary of the symbols used to define the algorithm.

Instrument count related parameters:

$$C = \text{instrument count} \quad (1)$$

$$C_0 = \text{dark or switch count} \quad (2)$$

$$C_{rel} = \text{relative instrument count} \quad (3)$$

Calibration slope-related parameters:

$$S = \text{calibration slope} \quad (4)$$

$$S_0 = \text{calibration slope at launch} \quad (5)$$

$$S_1 = \text{calibration parameter for } t \quad (6)$$

$$S_2 = \text{calibration parameter for } t^2 \quad (7)$$

$$t = \text{time in years since launch} \quad (8)$$

$$BT = \text{Brightness Temperature} \quad (9)$$

Reflectance related parameters:

$$R_u = \text{reflectance unadjusted for sun-earth distance or solar zenith angle} \quad (10)$$

$R$  = reflectance adjusted for sun-earth distance and solar zenith angle (11)

$\theta$  = solar zenith angle (12)

$D_{se}$  = sun-earth distance (13)

$PRT$  = Platinum Resistance Thermometer (14)

$T_{PRT}$  = blackbody temperature of the PRT (15)

$T_{BB}$  = Internal blackbody temperature (16)

$SW$  = smoothing weight (17)

$N_{BB}$  = radiance for the internal blackbody (18)

$N_S$  = radiance for the cold space (19)

$C_{BB}$  = Mean count values of the internal blackbody (20)

$C_S$  = Mean count values of the cold space (21)

$N_{LIN}$  = Linear radiance estimate (22)

$N_{COR}$  = Non linear correction of radiance (23)

### 1.3 Document Maintenance

Table 1 defines the versions of the APP CDR product release, the corresponding software package, and the C-ATBD. The Production software package is maintained at NCEI Subversion version control system.

**Table 1. Versions of the APP CDR product release, software, and the C-ATBD.**

Release Date	Product Version	Software Version	C-ATBD Version	Subversion Branch	Remarks
2015-09-01	V01	V01	V1.0	TBD	Initial draft
2019-01-15	V02	V02	V2.0		C-ATBD update

### 1.4 Improvements in APP v2.0

Version 2.0 of the APP fundamental climate data record has two important improvements: (1) the calibration uses the same code of the Clouds from AVHRR Extended (CLAVR-x)

processing system and the AVHRR PATMOS-x (Pathfinder Atmosphere-Extended) calibration available at [https://svn.ssec.wisc.edu/repos/cloud\\_team\\_clavrx/trunk/](https://svn.ssec.wisc.edu/repos/cloud_team_clavrx/trunk/) (Foster and Heidinger 2013), with the latest calibration coefficients of May 2018 for improved accuracy and efficiency, and (2) the entire data record (1982 – present) has been reprocessed for consistency. One minor update is the reflectance channel calibration in section 3.4.1.1, solar-earth distance factor is included. In v1.0, we took the same calibration approach of CLAVR-x and PATMOS-x, but wrote our code in another computer language, and got very similar results as CLAVR-x and PATMOS-x except non-negligible differences in visible channel reflectance. While the changes in v2.0 are significant for the dataset, the foundation of the algorithm remains the same, so only minor changes have been made to this C-ATBD.

## 2. Observing Systems Overview

### 2.1 Products Generated

The APP product is an FCDR comprised of calibrated and navigated AVHRR channel data (reflectances of visible channels and brightness temperatures of thermal channels), viewing and illumination geometry (sensor scan angle, solar zenith angle, and sun-sensor relative azimuth angle), Universal Coordinated Time (UTC) of the data acquisition, and a surface type mask. The data includes twice-daily composites on a 5 km Equal-Area Scalable Earth (EASE)-Grid over both poles, the Arctic and Antarctic, from 1982 to the present. The daily APP composites are centered on local solar times (LST) of 04:00 and 14:00 (high sun, but could be nighttime for some polar areas in winter) for the Arctic and 02:00 and 1400 for the Antarctic. The purpose of compositing based on local solar time rather than synoptic (UTC) time is to capture the diurnal cycle at all locations throughout the Arctic and Antarctic. Each composite is composed of as many as 23 orbits from the previous day to the next day (i.e. +/- 1 day), depending on the longitude of a pixel. APP covers the north polar region (Arctic) from 48.4 degrees northward, and the south polar region (Antarctic) from -53.2 degrees southward.

### 2.2 Instrument Characteristics

The series of NOAA Polar Orbiting Environmental Satellites (POES) started with TIROS-N (launched in October 1978), and continued with NOAA-A (renamed NOAA-6), NOAA-C (NOAA-7), NOAA-E (NOAA-8), NOAA-F (NOAA-9), NOAA-G (NOAA-10), NOAA-H (NOAA-11), NOAA-D (NOAA-12), NOAA-I (NOAA-13), NOAA-J (NOAA-14), NOAA-K (NOAA-15), NOAA-L (NOAA-16), NOAA-M (NOAA-17), NOAA-N (NOAA-18), MetOp-A, NOAA-N' (NOAA-19), and MetOp-B (Table 2) (Kidwell et al. 1995, 2009). The continuity of the instrument payload onboard the NOAA POES series provide an uninterrupted flow of global environmental information for establishing long-term data sets for climate monitoring. Table 2 provides some basic details associated with each of the NOAA POES series.

**Table 2: NOAA POES series**

Satellite Number	Launch Date	Ascending Node <sup>1</sup>	Descending Node	Service Date <sup>2</sup>
TIROS-N	10/13/78	1500	0300	10/19/78 – 1/30/80
NOAA-6	06/27/79	1930	0730	06/27/79 – 1/16/86
NOAA-7	06/23/81	1430	0230	08/24/81 – 2/01/85
NOAA-8	03/28/83	1930	0730	05/03/83 – 0/31/85
NOAA-9	12/12/84	1420	0220	02/25/85 – 1/07/88
NOAA-10	09/17/86	1930	0730	11/17/86 – 9/16/91
NOAA-11	09/24/88	1340	0140	11/08/88 – 6/16/04
NOAA-12	05/14/91	1930	0730	09/17/91 – 8/10/07
NOAA-14	12/30/94	1340	0140	04/10/95 – 5/23/07
NOAA-15	5/13/98	1930	0730	12/15/98 - present
NOAA-16	09/21/00	1400	0200	03/20/01 - present
NOAA-17	06/24/02	2200	1000	10/15/02 - 4/10/13
NOAA-18	05/20/05	1400	0200	08/30/05 - present
NOAA-19	02/06/09	1400	0200	06/02/09 - present
MetOp A <sup>3</sup>	10/19/06	2130	0930	06/20/07 - present
MetOp B <sup>3</sup>	09/17/12	2130	0930	04/24/13 - present

<sup>1</sup>An ascending node would imply a northbound Equatorial crossing while a descending node would imply a southbound Equatorial crossing.

<sup>2</sup>Service date is according to Kidwell et al. (1995) and POES Status at Office of Satellite Operations, NESDIS. Information from the latter is used if there is any discrepancy between these two.

<sup>3</sup>Operated by European Space Agency (ESA) and is part of EUMETSAT's Polar System (EPS).

The AVHRR is one of a few instruments that fly on all NOAA POES satellites. The AVHRR instruments onboard TIROS-N, NOAA-6, NOAA-8, and NOAA-10 are designated as AVHRR/1, which has only four spectral channels. The AVHRR onboard NOAA-7, NOAA-9, NOAA-11, and NOAA-14 are designated as AVHRR/2, which operates in five spectral channels. A version of the AVHRR with six spectral channels, AVHRR/3, is used on NOAA-15 and beyond. Channel 3a, with central wavelength at 1.61  $\mu\text{m}$ , operates in the daylight part of the orbit while channel 3b operates in the night portion of the orbit. Channel 3a and channel 3b cannot operate simultaneously. The specifications of the AVHRR channels are listed in Table 3.

The instrument scans in the cross-track direction with a field-of-view (FOV) of  $\pm 55.37^\circ$  from nadir and has an instantaneous FOV (IFOV) of 1.1 km at nadir (1.3-1.4 milliradians by 1.3-1.4 milliradians for all channels). The full resolution AVHRR data are stored and processed in the High Resolution Picture Transmission (HRPT) and Local Area Coverage (LAC) outputs. The full resolution data is also processed onboard the satellite into Global Area Coverage (GAC). To produce GAC data, four out of every five samples along the scan line are used to compute one average value and the data from only every third scan line are processed. This yields a 1.1 km by 4 km resolution at the subpoint with a 3.3 km gap between pixels across the scan line at nadir. Generally, the GAC data are considered to have a 4 km resolution. Details of the AVHRR instruments and data can be found in Kidwell et al. (1995, 2009).

**Table 3: Spectral specifications of AVHRR/1, /2, and /3**

Channel	TIROS-N	NOAA-6,8,10	NOAA-7,9,11,12,14	NOAA-15 and onward	HRPT nadir resolution (km)	GAC nadir resolution (km)
	AVHRR/1	AVHRR/1	AVHRR/2	AVHRR/3	1.1	4.0
1	0.55-0.90 $\mu\text{m}$	0.58-0.68 $\mu\text{m}$	0.58-0.68 $\mu\text{m}$	0.58-0.68 $\mu\text{m}$	1.1	4.0
2	0.725-1.10 $\mu\text{m}$	0.725-1.10 $\mu\text{m}$	0.725-1.10 $\mu\text{m}$	0.725-1.00 $\mu\text{m}$	1.1	4.0
3A				1.58-1.64 $\mu\text{m}$	1.1	4.0
3B	3.55-3.93 $\mu\text{m}$	3.55-3.93 $\mu\text{m}$	3.55-3.93 $\mu\text{m}$	3.55-3.93 $\mu\text{m}$	1.1	4.0
4	10.50-11.50 $\mu\text{m}$	10.50-11.50 $\mu\text{m}$	10.30-11.30 $\mu\text{m}$	10.30-11.30 $\mu\text{m}$	1.1	4.0
5	Ch4 repeated	Ch4 repeated	11.50-12.50 $\mu\text{m}$	11.50-12.50 $\mu\text{m}$	1.1	4.0

The AVHRR GAC data is used to generate the APP FCDR. Significant variations in the equatorial crossing time (ECT) of a satellite will impact the accuracy in generating a consistent time series. There have been considerable drifts in the NOAA POES ECTs, as shown in Figure 1. The APP is composited at 0400 and 1400 local solar time (LST) for the Arctic, and 0200 and 1400 LST for the Antarctic. Only the NOAA satellites listed in Table 4 are used in the creation of APP, because these satellites carry AVHRR instruments with all five channels and the ECT of these satellites are relatively consistent. Five-channel AVHRRs are needed for most geophysical parameter retrieval, so the NOAA satellites before NOAA-7 and even-numbered satellites before NOAA-11 are not included. It should be noted that

NOAA-16 has Channel 3A/3B switch, while NOAA-18 has only Channel 3B after August 5, 2005.

**Table 4: NOAA POES satellites used in APP.**

NOAA satellite	Time range	Note
NOAA-7	01/01/82 – 12/31/84	
NOAA-9	01/01/85 – 11/07/88	
NOAA-11	11/08/88 – 12/31/94	
NOAA-14	01/01/95 – 12/31/00	
NOAA-16	01/01/01 – 08/09/05	NOAA-16 has Channel 3A/3B switching
NOAA-18	08/10/05 – 12/31/2014	On 08/05/05, automatic 3A/3B channel switching was disabled. Channel 3B is permanently on NOAA-18.
NOAA-19	1/1/2015-present	

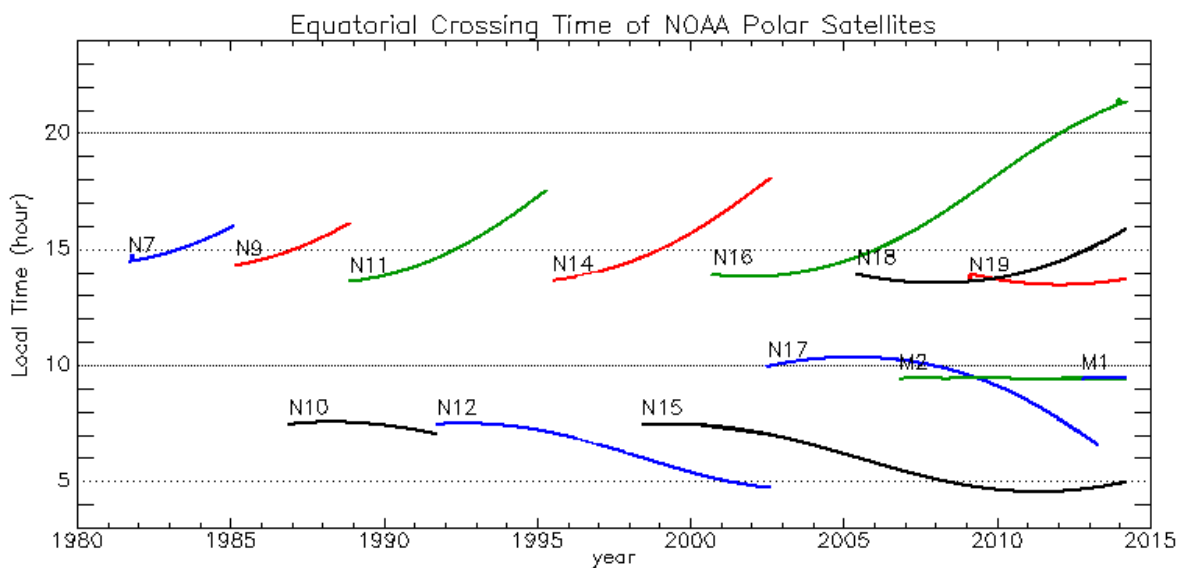


**Figure 1: Equatorial crossing time of NOAA POES. (Figure is from [www.star.nesdis.noaa.gov/smcd/emb/vci/VH/vh\\_avhrr\\_ect.php](http://www.star.nesdis.noaa.gov/smcd/emb/vci/VH/vh_avhrr_ect.php). The original ECT data are from [www.ospo.noaa.gov/Products/ppp/navpage.html](http://www.ospo.noaa.gov/Products/ppp/navpage.html).)**

## **3. Algorithm Description**

### **3.1 Algorithm Overview**

The generation of APP daily composites includes the following steps:

1. AVHRR GAC Level 1b data from NOAA POES from the previous day, current day, and the next day are acquired. Approximately 23 overpasses will potentially be used.
2. AVHRR GAC Level 1b data are calibrated following the steps in section 3.4.1 to obtain the visible channel reflectances and thermal channel Brightness Temperatures (BT).
3. AVHRR GAC Level 1b data are navigated following steps in section 3.2.3 to obtain accurate longitude/latitude and viewing angles.
4. Overpasses within a time window centered on 0400 and 1400 local solar time (LST) for the Arctic, and 0200 and 1400 LST for the Antarctic, are combined/composited based on sensor scanning angle and time difference from the target time.

The twice-daily composites that comprise the APP FCDR consist of AVHRR channel reflectances and brightness temperatures, sensor scan angle, solar zenith angle, sun-sensor relative azimuth angle, Universal Coordinated Time (UTC) of the data acquisition, and a surface type mask.

### **3.2 Processing Outline**

The four main steps used to generate the APP FCDR are outlined in Figure 2. Each step is explained in the following paragraphs.

## APP Processing Overview

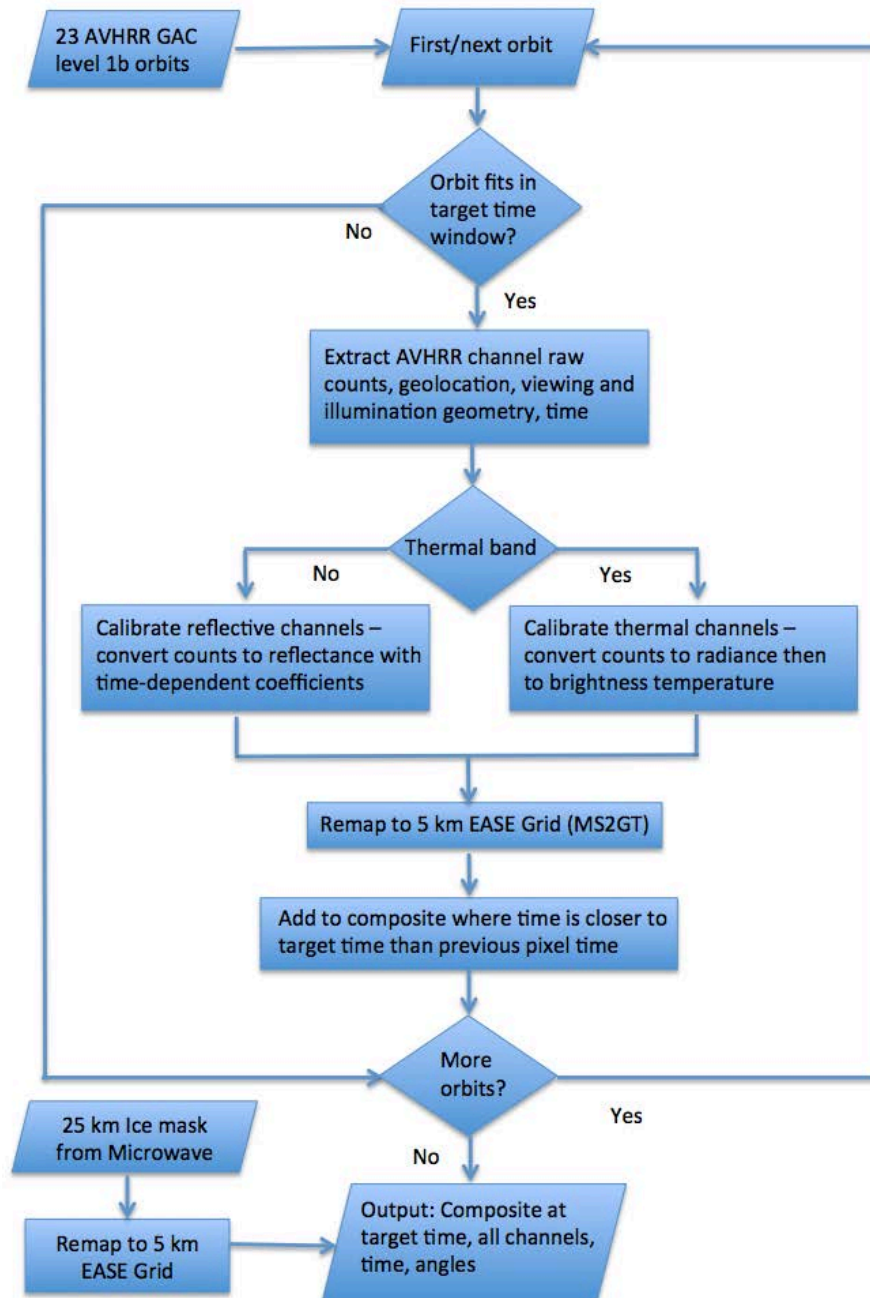


Figure 2: Flow chart of processing steps to generate APP from AVHRR GAC level 1b data for a single target time.

### 3.2.1 Data Ingest

Step 1 is data ingest. For a daily composite, AVHRR GAC level 1b data, at roughly 4 km spatial resolution, for all satellite overpasses with ending time after 12 UTC of the previous day, the current day, and starting time before 4UTC of the next day are acquired. The approximate number of overpasses that go into each of the twice-daily composites is 23.

### 3.2.2 Calibration

Step 2 is calibration. Calibration is described in section 3.4.1, *Physical and Mathematical Description*.

### 3.2.3 Navigation

Step 3 is navigation. Each scan line in AVHRR GAC level 1b data contains 409 viewed spots, but only 51 of those are geolocated in the level 1b data. The geolocations, longitude and latitude, of the 25th data sample and every 40th thereafter are included in the level 1b data by the Advanced Location Data System during the preprocessing of the data on the ground. A five-point Lagrangian interpolation is applied to derive the longitude/latitude for 2048 LAC pixels at 1.1 km resolution, from which the longitude/latitude of the 409 GAC pixels are extracted. For regions north of 85 degrees north or south of 85 degrees south, the interpolation is done in the Gnomonic Space (Sullivan and Jelenak, 2007). The viewing angles are all interpolated using linear interpolation.

### 3.2.4 Compositing

Step 4 is compositing. In this step, all calibrated overpasses are composited. There are two daily composites in the 5 km EASE Grid for both the Arctic and the Antarctic with dimensions N by N, where N is 1805 for Arctic and 1605 for the Antarctic. For the Arctic, the two composites are for target times of 0400 and 1400 Local Solar Time (LST), respectively. For the Antarctic the two target times are 0200 and 1400 LST.

Data in each overpass from the first three steps are remapped to the 5 km EASE Grid based on longitude/latitude. The grid is then filled with data from the various overpasses in the following way. First, only those pixels in the overpasses whose time is within 3 hour of the target time are considered. Second, a pixel in an overpass updates the composite image pixel if the sensor scan angle for that pixel is less than (closer to nadir) the one that was previously used.

This method minimizes the scan angle dependence of the daily composite at the possible expense of obtaining an observation further from the target time. This is reasonable because retrievals of many geophysical parameters are strongly dependent upon scan angle, with uncertainty typically increasing at large scan angles.

Each composite time utilizes up to 23 overpasses, 14 from the current day, 7 from the day before, and 2 from the day after. It should be noted that the composites are for local solar time, not a fixed synoptic (UTC) time.

## 3.3 Algorithm Input

### 3.3.1 Primary Sensor Data

Every overpass of AVHRR GAC level 1b from January 1, 1982 to the present for NOAA satellites listed in Table 4 is used to generate the APP. This data set can be ordered from the NOAA's Comprehensive Large Array-data Stewardship System (CLASS).

### 3.3.2 Ancillary Data

A surface mask is also included in the APP output. It is not needed for, and is not part of, the AVHRR processing but rather is included as it may be of value in some user applications. For years prior to 1995, the surface mask is generated as follows. The daily averaged Polar Gridded Brightness Temperature of Special Sensor Microwave/Imagers (SSM/I) onboard the Nimbus-7 Scanning Multichannel Microwave Radiometer (SMMR) and the Defense Meteorological Satellite Program (DMSP) were regrided to the 25 km EASE Grid. Surface type, including land, ice sheets, and ocean are then identified. Over oceans, the NASA Team Sea Ice Algorithm was used to generate first-year and multi-year ice concentrations. In some cases, atmospheric effects and wind roughening of the ocean cause false ice concentration retrievals over open ocean. Such areas will appear as incorrectly mapped areas of sea ice in the mask. Areas that consist of at least 50 percent multi-year ice are assigned the multiyear ice flag.

The multiyear ice estimate is subject to considerable error and uncertainty, particularly during periods when surface melt is likely (Cavalieri et al., 1999). At such times, characteristic multiyear ice emission properties are partially or completely hidden, and melt-freeze metamorphosis or other changes in the snow cover on sea ice may cause first-year ice to appear as a fraction of multi-year ice. Since thresholds were applied to the output from ice concentration, ice type, and snow depth algorithms, slight variations in the values yield a noisy appearance in the resulting binary flag images, particularly in spring and summer due to algorithm limitations. Over land, snow cover is detected with an SSM/I algorithm described in Goodison (1989). A gradient value (19 GHz horizontal polarization minus 37 GHz horizontal polarization) greater than zero indicates snow and the pixel is assigned a snow surface type. Special cases such as melting snow are not addressed in this mask. The SSM/I data have different coverage areas and thus the regriding process of the SSM/I leaves some areas without information over certain regions. The Near-Real-Time SSM/I EASE Grid Daily Global Ice Concentration and Snow Extent and Northern Hemisphere EASE Grid Weekly Snow Cover and Sea Ice Extent products from NSIDC were used to fill in the missing regions wherever possible. The resulting 5 km mask is over-sampled from the 25 km SSM/I data. Because coastal areas have a jagged appearance, a 5 km land mask is applied to the surface mask and the nearest appropriate surface type mask is used.

After the year 1995, the surface mask is from the Near-Real-Time SSM/I-SSMIS EASE Grid Daily Global Ice Concentration and Snow Extent, Version 4 (Nolin et al. 1998). This data set is in 25 km EASE Grid projection, which is then re-gridded to 5 km EASE Grid for APP.

In addition to the GAC files, AVHRR instrument files are used that contain instrument-specific data including the mean dark count and the calibration coefficients derived from Heidinger et al. (2010) and Molling et al. (2010). These files are maintained under version control software and available directly from Andrew Heidinger (Andrew.Heidinger@noaa.gov).

### 3.3.3 Derived Data

There are no derived parameters in APP beyond the calibrated and navigated reflectances and brightness temperatures. It is the primary input to the extended AVHRR Polar Pathfinder Product, APP-x. APP-x is described in a separate C-ATBD.

### 3.3.4 Forward Models

The Moderate resolution Imaging Spectroradiometer (MODIS) Swath-to-Grid Toolbox (MS2GT) is a set of software tools that reads HDF-EOS files containing swath data and produces flat binary files containing gridded data in a variety of map projections. MS2GT was originally written to map/grid MODIS data but it can be used with many types of satellite data. MS2GT consists of three Perl programs that make calls to several standalone IDL and C programs: mod02.pl which reads MOD021KM, MOD02HKM, or MOD02QKM Level 1b files, mod10\_l2.pl which reads MOD10\_L2 snow cover files, and mod29.pl which reads MOD29 sea ice files. All three Perl programs can optionally read MOD03 files for geolocation information. In addition, mod02.pl can extract ancillary data (such as illumination and viewing angles) from MOD03 files.

The MS2GT software is used to remap the calibrated AVHRR GAC level 1b data at 4 km spatial resolution to 5 km EASE Grid. In this application, IDL programs are written to prepare the inputs to MS2GT, and process the outputs of MS2GT.

## 3.4 Theoretical Description

APP has two daily composites derived from AVHRR GAC Level 1b data for both polar regions. The entire process consists of four main steps, extraction of the input data, calibration of the original data, navigation of each pixel of observations, and composition of all overpasses in three days as explained in details in section 3.2.

### 3.4.1 Physical and Mathematical Description

#### 3.4.1.1 Reflectance Channel Calibration

The calculation of calibrated reflectance is fairly simple. The basic order of operations is this for data from each of the three channels:

1. Read in raw count, dark count, angles, sun-earth distance, time, and navigation from Level1b file.
2. Read in constants from the instrument file.
3. Compare dark count to average dark count. Reject the

- observation if different by more than 5 counts.
4. Subtract dark count from the raw count to get relative count or subtract the switch count (the count at which the gain switches) from the raw count to get high gain relative count.
  5. Compute days since launch using time (1b) and launch date (instrument file).
  6. Compute calibrated slope using days since launch and calibration parameters (instrument file).
  7. Multiply relative count by calibrated slope to get calibrated reflectance.
  8. Correct for sun-earth geometry using sun-earth distance and solar zenith angle.
  9. Correct navigation.
  10. Write reflectances and related variables (angles, time) to output file.

Reflectance is obtained from an electronic instrument in the following way: The instrument's sensors are sensitive to a certain band of wavelengths. The AVHRR instrument has sensors that are capable of measuring energy in the visible (Channel 1), the near infrared (Channel 2), and the middle infrared (Channel 3a). The spectral response functions for these three AVHRR channels can be found at <http://www.star.nesdis.noaa.gov/smcd/spb/calibration/avhrr/nrf.html>. The electronics convert the energy sensed in the band to a digital count. The greater the magnitude of this energy (signal), the larger the count. The older AVHRRs, AVHRR/1 and AVHRR/2, have a linear signal count response or gain, while the AVHRR/3s have a two-segment linear gain. The sensor also points into deep space during one part of each scan to record a dark count. The dark count is used to anchor the reflectance equation at zero. A calibration slope is used to convert the counts to reflectance units. This slope includes any factors involved: spectral response function, solar constant, instrument gain, etc.

$$R_u = S * (C - C_0)$$

Where  $R_u$  is the reflectance unadjusted for sun-earth distance or solar zenith angle,  $S$  is the calibration slope,  $C$  is the instrument count, and  $C_0$  is the dark count. For AVHRR/3, counts below the switch count use the above equation with the low gain slope. For counts above the switch count, the switch count is used for  $C_0$ , and the high gain slope applied.

Some calibrations, such as those published in the polar orbiter data (POD) and NOAA KLM Guides, use a slope and intercept directly on the count and do not use the dark count. Using or not-using the dark count is built into any calibration, and is neither right nor wrong, as long as the calibration can return a zero reflectance for counts below some threshold.

The AVHRR calibration is originally done pre-launch, but once the instrument is launched, this calibration typically changes (immediately, due to launch conditions, and over time as the instrument ages). After launch, the instrument can only be calibrated indirectly, as there is no on-board calibration source for Channels 1, 2, and 3A. The computation of the calibration slopes,  $S$ , is described in section 3.4.4 and in Heidinger et al. (2010) and Molling et al. (2010). An ATBD for the Channel 1 and 2 calibrations is also available at <https://gsics.nesdis.noaa.gov/wiki/Development/AtbdCentral>.

### 3.4.1.2 Thermal Channel Calibration

The steps of calibration for the AVHRR thermal bands, channel 3b, channel 4 and channel 5, are mainly following the steps listed in chapter 7.1.2.4 in Kidwell et al. (2009). They are used for both AVHRR pre-KLM and KLM.

1. The temperature of the internal blackbody target is measured by four platinum resistance thermometers (PRT). On each scanline, a different PRT is sampled and three readings are recorded; on the fifth scanline all three PRT values for each PRT are set equal to 0 to indicate that a set of four PRTs has just been sampled. The temperature of each PRT,  $T_{PRT}$ , is calculated based on  $C_{PRT}$  with coefficients  $d_1, d_2, d_3, d_4$ , where  $C_{PRT}$  is the mean of the three readings of each PRT.

$$T_{PRT} = d_0 + d_1 C_{PRT} + d_2 C_{PRT}^2 + d_3 C_{PRT}^3 + d_4 C_{PRT}^4$$

The coefficients  $d_0, d_1, d_2, d_3, d_4$ , are available from tables in Appendix D in Kidwell et al (2009) and also included in the ancillary files of this algorithm. The internal blackbody temperature  $T_{BB}$  is then derived with consideration of  $T_{BB}$  values from previous calculations.

$$T_{BB} = (1 - SW)T_{BB1} + SW * T_{BB2}$$

$T_{BB1}$  is the blackbody temperature of the previous scan line, and  $T_{BB2}$  is the blackbody temperature of the current scan line.  $SW$  is the smoothing weight set at 0.2.

2. The radiance  $N_{BB}$  sensed in each thermal AVHRR channel for the internal blackbody at temperature  $T_{BB}$  is calculated with a rapid Planck calculation using a lookup table approach. Cold space radiance  $N_S$  is a constant for each satellite, and is read in from ancillary files.

3. Mean count values of the 10 AVHRR views of the internal blackbody and cold space targets,  $C_{BB}$  and  $C_S$  are calculated with consideration of values from previous calculations with a smoothing weight of 0.2. The linear slope  $C_E$  and intercept  $I$  to convert the count output of AVHRR viewing the Earth targets to linear radiance estimate  $N_{LIN}$  is

$$N_{LIN} = M * C_E + I$$

where  $M = (N_S - N_{BB}) / (C_S - C_{BB})$ , and  $I = N_S - M * C_S$ .

Nonlinear response of radiance is added to  $N_{LIN}$  to get the final radiance  $N_E$ ,

$$N_E = N_{LIN} + N_{COR}$$

The nonlinear correction of radiance is based on the linear radiance as

$$N_{COR} = b_0 + b_1 N_{LIN} + b_2 N_{LIN}^2$$

where  $b_1$ ,  $b_2$ , and  $b_3$  are coefficients based on post-launch research work (Kidwell et al. 2009), and are read from the ancillary files. All the coefficients are included in the instrument constant files discussed in section 3.3.2.

The corrected radiance is then converted to brightness temperatures with a rapid Planck calculation using a lookup table approach.

### 3.4.2 Data Merging Strategy

Data merging, i.e., compositing, is described in section 3.2.4.

### 3.4.3 Numerical Strategy

Not Applicable.

### 3.4.4 Calculations

Once the channel counts are read in, the space count or switch count is subtracted to form a relative count,  $C_{rel}$ , and then the calibration is applied. The calibration converts raw counts to reflectance. The calibration parameters are a function of time since launch:

$$S(t) = S_0 (100 + S_1 t + S_2 t^2) / 100$$

where  $S$  is the calibration slope (reflectance in %/count),  $S_0$ ,  $S_1$ , and  $S_2$  are the calibration terms, and  $t$  is the time in years since launch. If the instrument is dual gain, the raw absolute count is compared to the gain switch. If the count is less than the switch, the low gain calibration parameters are applied; if above, the high gain calibration is applied. The calibration parameters  $S_0$ ,  $S_1$ , and  $S_2$ , respectively, are in Table 5.  $S_0$  is considered to be the calibrated slope at launch, while  $S_1$  and  $S_2$  are the time-dependent degradation coefficients. These coefficients have been updated periodically after the paper published in 2010, and the latest coefficients are included in the ancillary files in this algorithm package.

**Table 5: Calibration slope parameters for AVHRR channels 1 and 2 (Heidinger et al., 2010).**

Satellite	Channel 1			Channel 2		
	$S_0$	$S_1$	$S_2$	$S_0$	$S_1$	$S_2$
TIROS-N	0.105	27.015	-12.876	0.121	10.709	-0.643
NOAA-6	0.088	47.977	-16.122	0.077	97.301	-32.590
NOAA-7	0.117	3.635	0.045	0.119	6.579	-0.620
NOAA-8	0.116	14.177	-2.729	0.132	12.611	-2.713
NOAA-9	0.110	3.242	0.793	0.117	2.365	0.155
NOAA-10	0.108	9.819	-1.615	0.127	5.201	-0.707
NOAA-11	0.114	0.022	0.091	0.116	0.299	0.045
NOAA-12	0.123	2.624	-0.116	0.147	1.191	-0.041
NOAA-14	0.120	5.034	-0.489	0.147	0.023	0.311
NOAA-15	0.121	0.447	-0.060	0.135	0.035	0.007
NOAA-16	0.112	0.306	0.025	0.116	0.586	0.036
NOAA-17	0.115	1.707	-0.151	0.130	3.117	-0.265
NOAA-18	0.111	3.068	-0.443	0.119	4.541	-0.611
NOAA-19	0.112	-5.985	-8.687	0.117	2.263	0.748
Metop-A	0.111	1.797	-0.352	0.127	2.149	-0.225

### 3.4.5 Look-Up Table Description

Other than the instrument files, discussed in Section 3.3.2, the only look-up tables used are clock correction tables stored in the code. These were obtained from the University of Miami (see [http://yyy.rsmas.miami.edu/groups/rrsl/pathfinder/Processing/proc\\_index.html](http://yyy.rsmas.miami.edu/groups/rrsl/pathfinder/Processing/proc_index.html)). These are used to correct navigation only. They do not alter reflectance values.

### 3.4.6 Parameterization

Not Applicable.

### 3.4.7 Algorithm Output

This algorithm generates the APP composites at 5 km EASE Grid twice daily over both poles, Arctic and Antarctic, from 1982 to the present. The twice daily composite consists of five AVHRR channel data, sensor scanning angle, solar zenith angle, sun-sensor relative azimuth angle. Complimentary data include the Universal Coordinated Time (UTC) of the data acquisition, and surface type mask. The daily APP composites are centered on local solar times of 1400 (high sun, but could be nighttime for some polar areas in winter) and 0400 for the Arctic or 0200 for the Antarctic. APP covers the Arctic from 48.4° N to the North Pole, and the Antarctic from -53.2° S to the South Pole. All the daily data at each LST for each pole are stored in one netCDF file, so there are four files for each year. The output details are listed in Table 6.

**Table 6: APP output**

Name	File format and size	Content	Note
APP_n005_####_0400.nc	netCDF, 22 gb (6gb)	Longitude	Degree, -180 to 180
APP_n005_####_1400.nc	22 gb (6gb)	Latitude	Degree, positive for NH
APP_s005_####_0200.nc	17 gb (4gb)	Julian day	
APP_s005_####_1400.cn	17 gb (4gb)	Ch1 reflectance	%
####: year, e.g. 2000	uncompressed (compressed)	Ch2 reflectance	%
		Ch3 BT/reflectance	K/%
		Ch4 BT	K
		Ch5 BT	K
		Sensor scanning angle	Degree
		Solar zenith angle	Degree
		Sun-sensor relative azimuth angle	Degree
		UTC of observation	hhmmss

## 4. Test Datasets and Outputs

### 4.1 Test Input Datasets

For the Arctic composite, July 1 data for every year from 1982 to 2013 are used as the test datasets, both visible channel reflectance and thermal channel BT. For the Antarctic composite, January 1 data of every year from 1982 to 2013 are used. There is a total of 32 days of data available for both poles. The input data is the AVHRR GAC level 1b data from the University of Wisconsin Space Science and Engineering Center (SSEC) Data Center; they are identical to those data archived at NOAA CLASS. Daily APP composites are generated using these test input datasets.

### 4.2 Test Output Analysis

#### 4.2.1 Reproducibility

Pixel-to-pixel comparisons of each of the APP output variables to those produced in test cases during the algorithm development process are performed to verify the output. Two examples of the output are shown in Figures 3 and 4. No discrepancies were found.

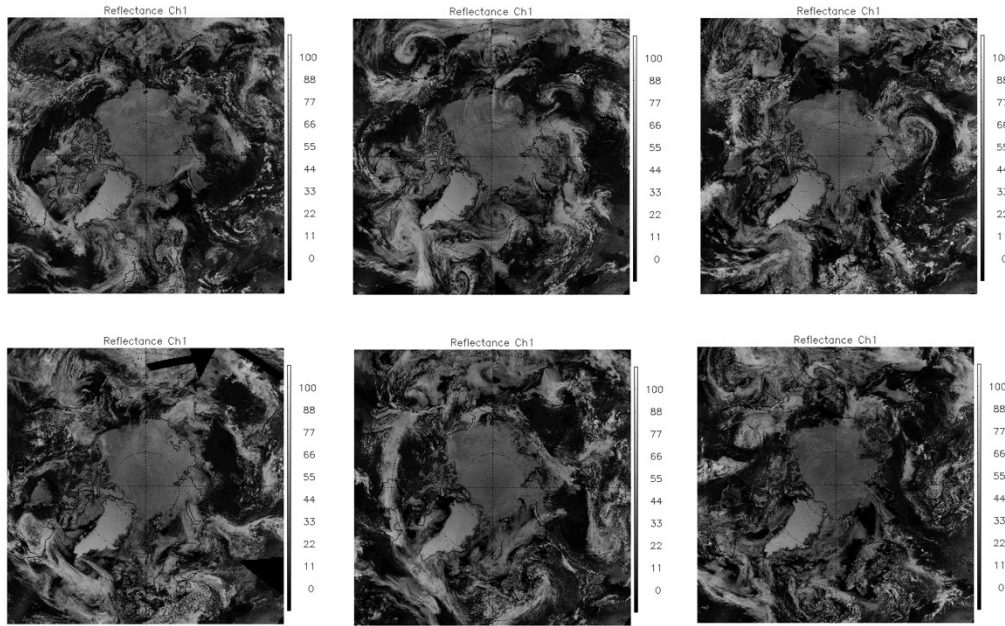


**Figure 3: APP channel 1 reflectance (%) at 1400 LST of the Arctic on July 1 of the year 1982, 1986, 1989, 1996, 2002, and 2007.**

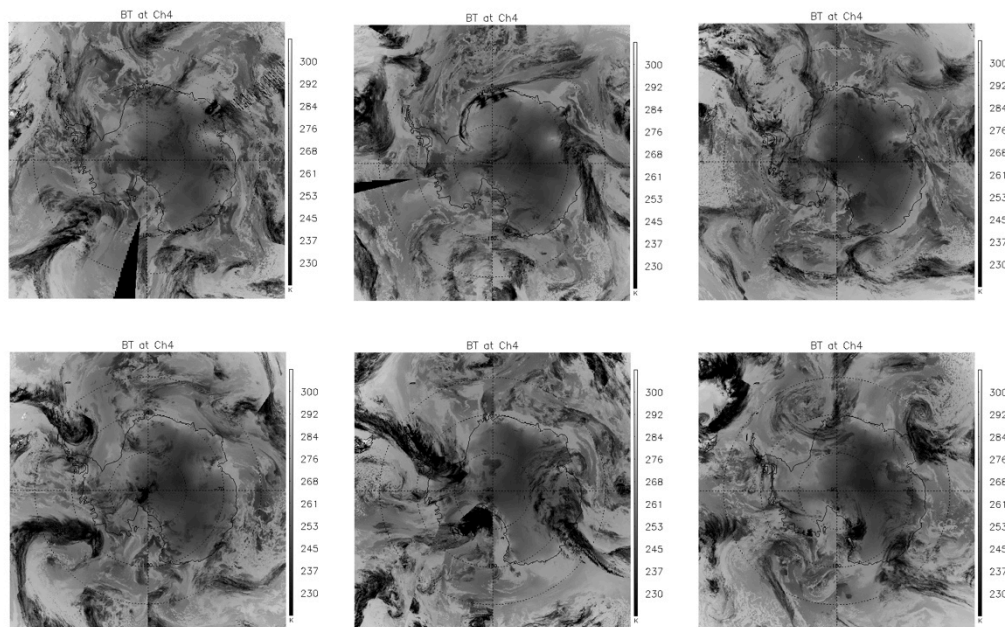


**Figure 4: APP channel 4 BT (K) at 1400 LST of the Antarctic on January 1 of the year 1982, 1986, 1989, 1996, 2002, and 2007.**

## 4.2.2 Precision and Accuracy

Precision of reflectance starts with the fact that the input counts are 10bit. The full range in reflectance, 0 to about 110% (reflectances greater than 100% are possible) is represented by counts ranging from 0 to 1023, implying that the counts themselves allow a precision of about 0.1% in reflectance units. However, the calibration slope for each AVHRR determines the precision for that particular instrument and range. Channel 1 slopes at launch (and therefore precision values) range from 0.09 to 0.12 for single gain AVHRRs (TIROS-N through NOAA-14). Dual-gain AVHRRs have a higher precision in the low reflectance gain region and lower precision in the high gain region. This ranges (in reflectance units of %) for Channel 1, low gain, from 0.05 to 0.06, and high gain 0.17 to 0.20. Channel 2 precision at launch ranges from 0.08-0.13 for single gain, and 0.05-0.06 and 0.17-0.20 for low and high gain, respectively. Channel 3a is only present on dual gain AVHRRs, and precision at launch ranges from 0.02-0.03 for low gain and 0.18-0.22 for high gain. Slopes and precision values tend to increase after launch. The maximum slopes/precision values are 0.14 for Ch1, 0.22 for Ch2, and 0.24 for Ch3a.

Accuracy, on the other hand is determined by both the calibration and the method of producing the Level2b data. The accuracy of the calibration procedure with respect to MODIS Collection 5 is 2% for Channel 1 and 3% for Channel 2. Channel 3a's accuracy is 3%. These accuracies are for the reflectance value itself. Thermal channel calibration errors are typically in the range 0.03 – 0.3K at 300K, depending on the channel and radiometer. The noise increases as temperature decreases (Trishchenko et al., 2002).

Level1b data contain navigation errors from 2 to 10 km (Heidinger et al. 2002). These errors introduce uncertainty in the actual location of each reflectance value of up to 20km. Improved orbit stabilization of the satellites bearing AVHRR/3s will contribute to higher accuracy reflectances due to higher accuracy navigation.

Additional comparisons to MODIS were done by generating a MODIS composite dataset similar in form to APP. Daily MODIS composites were generated at 0400 and 1400 LST at 5 km EASE Grid resolution using 1 km resolution MODIS Aqua data at similar channels as AVHRR channels, including MODIS channel 1 (0.62-0.67  $\mu\text{m}$ ), channel 2 (0.841-0.876  $\mu\text{m}$ ), channel 22 (3.929-3.989  $\mu\text{m}$ ), channel 31 (10.78-11.28  $\mu\text{m}$ ), and channel 32 (11.77-12.27  $\mu\text{m}$ ). A comparison of APP and MODIS Aqua composites provides a rough estimate of the precision and accuracy of APP composites. Figure 5 provides one example of such a comparison. For this case, the bias and standard deviation between APP and MODIS Aqua composites at 1400 LST of Arctic are -3.31% and 10.18% for channel 1, and 0.92 K and 8.21 K for channel 4. Other cases yield similar statistics. It should be noted that these two composites are at somewhat different wavelengths, times, and viewing angles. Differences of this magnitude are therefore reasonable.

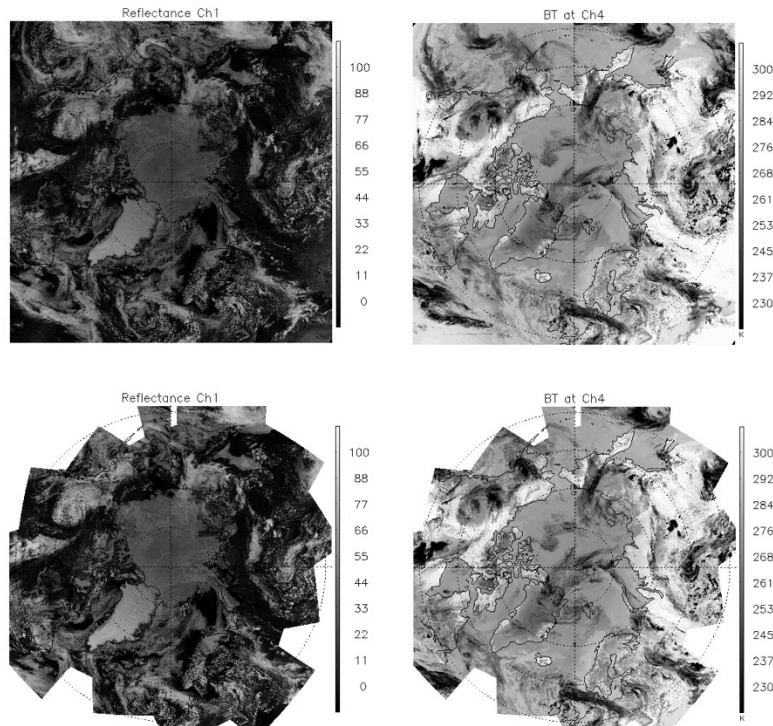


**Figure 5: Channel 1 reflectance (%) and channel 4 BT (K) at 1400 LST of the Arctic on July 1 of the year 2007 from APP (upper row) and MODIS Aqua (lower row).**

### 4.2.3 Error Budget

Table 7 contains a summary of the known errors in calibration and navigation of AVHRR GAC data. See Section 4.2.2 for additional details and references.

**Table 7: Summary of Errors in AVHRR Ch1, Ch2, and Ch3a reflectance data set.**

Error	Magnitude of Error
Reflectance channel calibration errors	Ch1: 2%, Ch2: 3%, Ch3a: 3%
Thermal channel calibration error	0.03 – 0.3K at 300K
Level1b navigation error	Up to 20 km

## 5. Practical Considerations

## 5.1 Numerical Computation Considerations

Not Applicable.

## 5.2 Programming and Procedural Considerations

On a Linux machine, running on a single 2.6 GHz Opteron™ Processor 4180, it takes 16 minutes to generate daily composites at two times per day for both poles. Prior to 2005, the codes are in Bash shell scripts and C programs.

## 5.3 Quality Assessment and Diagnostics

Current quality assessment is limited to out-of-range value detection and the number of missing (unfilled) pixels in the grid. Additional quality assessment and diagnostic statistics are being considered for future versions of the data.

## 5.4 Exception Handling

Error messages are recorded for every step of the processing.

## 5.5 Algorithm Validation

The calibration methods are provided by NOAA and have been validated by NOAA. Composite images have been “spot checked” manually against calibrated swath data and no discrepancies have been found.

## 5.6 Processing Environment and Resources

Before the year 2005, shell script and C programs are used to process the data on an x86\_64 m64 server running the red hat Linux or CentOS operating system. After the year 2005, b shell script and IDL version 8.0 are used to process the data on an x86\_64 server running the red hat Linux or CentOS operating system. The input for daily composite is around 2.4 GB, and output for annual data is 78 GB without compression.

## 6. Assumptions and Limitations

Not Applicable

### 6.1 Algorithm Performance

The performance of the calibration method has been documented elsewhere (Heidinger et al., 2010; Molling et al., 2010). On the inter-satellite differences are addressed here. We have examined the time series of AVHRR brightness temperatures and reflectances for NOAA-7, -9, -11, and -14 over the period of 1982-1999. If the calibration procedures are effective, and if the changes in viewing/illumination geometry are small, there should be no obvious discontinuities across satellite boundaries. We use Barrow, Alaska as a “calibration” location because surface temperature measurements show no significant trend over the study period. Figure 6 shows the time series of channel 4 brightness

temperatures for 1982-1999, a period covering four satellites (NOAA-7, -9, -11, and -14). The monthly average brightness temperatures were generated for a 275 x 275 km<sup>2</sup> area around Barrow at a local solar time of about 1400. There is no obvious change from one satellite to the next that could be attributed to differences in calibration. (Note: From NOAA-11 to NOAA-14 there are no data available from September 14, 1994 to January 18, 1995.)

Figures 7 and 8 show the time series of AVHRR channel 4 brightness temperatures based on daily observations at Barrow. They clearly indicate that the change in satellites caused only a very small change of the brightness temperature, significantly less than the daily variation. The APP-x data set exhibits very good infrared channel intercalibration between NOAA-7, -9, -11, and -14. Figure 9 shows a time series of monthly average surface skin temperatures from the APP-x data set. The retrieval algorithm adjusts for viewing angle, so that orbital drift is even less of an issue than with brightness temperatures alone. There is no obvious discontinuity from one satellite to the next.

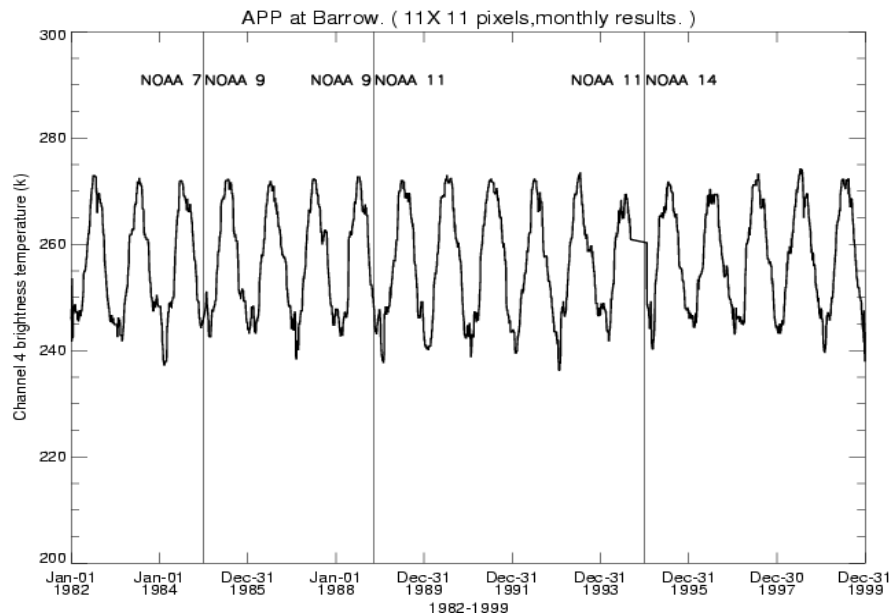


**Figure 6: Time series of monthly average AVHRR channel 4 brightness temperatures from January 1, 1982 to December 31, 1999 at Barrow, Alaska for 1400 local solar time. Note: there are no data available from September 14, 1994 to January 18, 1995.**

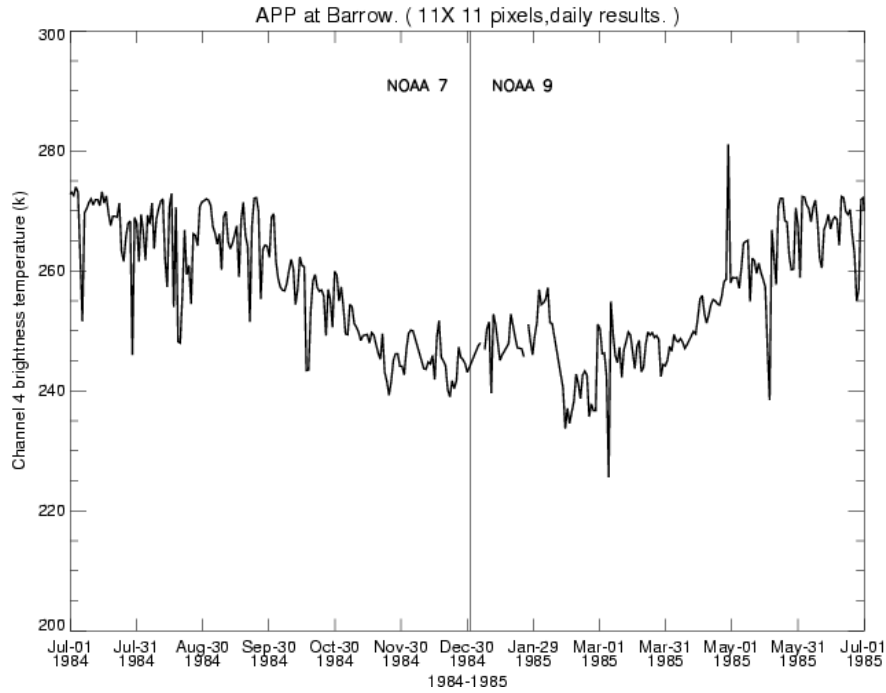


**Figure 7: Time series of daily AVHRR channel 4 brightness temperatures from July 1, 1984 to July 1, 1985 at Barrow, Alaska for 1400 local solar time covering the change from NOAA-7 to NOAA-9 (vertical line).**

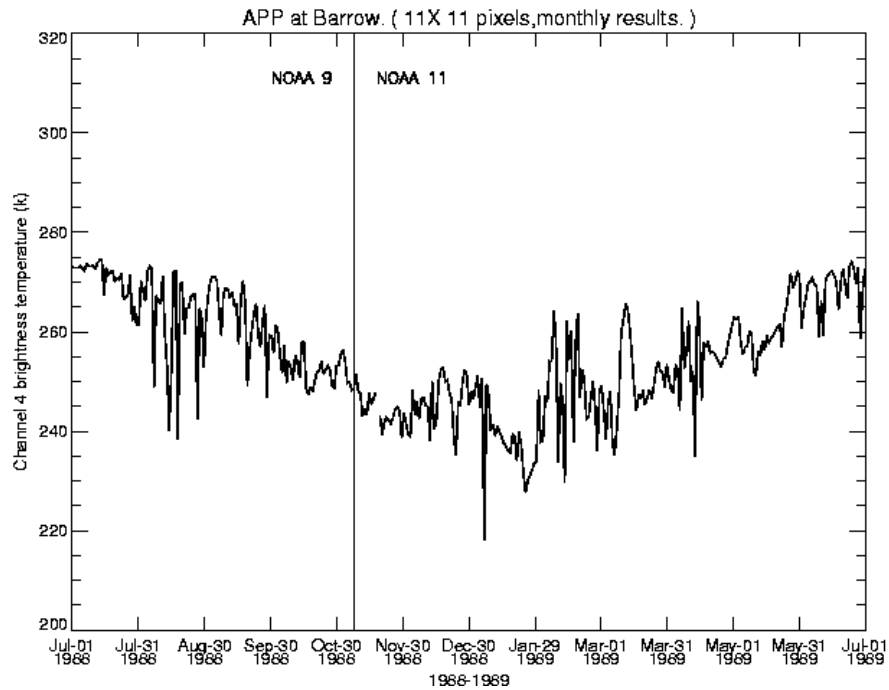


**Figure 8: Time series of daily AVHRR channel 4 brightness temperatures from July 1, 1988 to July 1, 1989 at Barrow, Alaska for 1400 local solar time, covering the change from NOAA-9 to NOAA-11 (vertical line).**

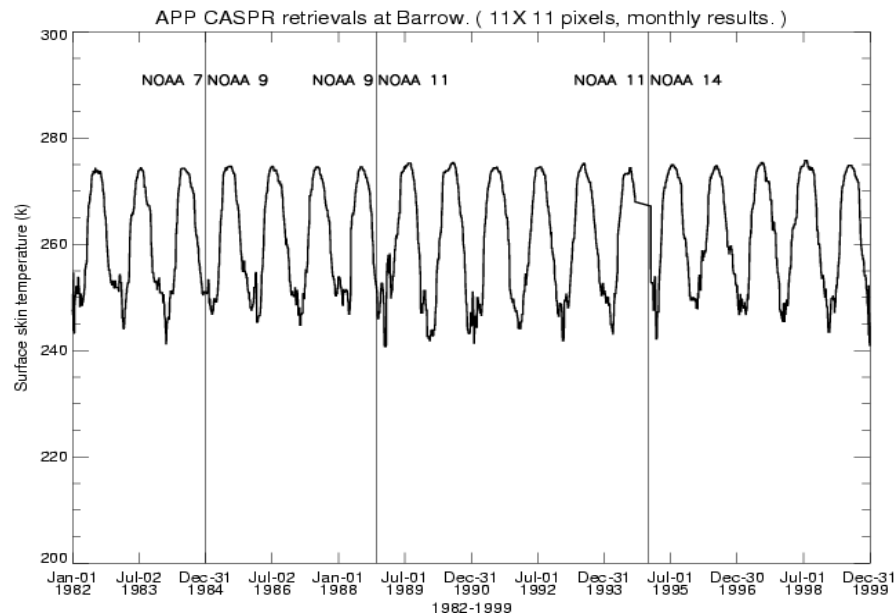


**Figure 9: Time series of monthly average surface skin temperatures from January 1, 1982 to December 31, 1999 at Barrow, Alaska for 1400 local solar time. Note: there are no data available from September 14, 1994 to January 18, 1995.**

Because the NOAA satellite transitions occurred during the Northern hemisphere winter, Vostok, Antarctica was used to examine the AVHRR visible channels. Due to orbital drift and different equator crossing times, significant changes in visible channel reflectances can be expected from one satellite to the next. Figure 10 shows the time series of the AVHRR channel 2 reflectances from July 1, 1984 to July 1, 1985 at 1400 local solar time over a 275 x 275 km<sup>2</sup> area around Vostok. There is a rather abrupt change at the time of the satellite transition.

Figures 11 and 12 show the time series of the sensor scan angles and solar zenith angles from July 1, 1984 to July 1, 1985 during the transition from NOAA-7 to NOAA-9. It shows that the solar zenith angle difference is small, but that the scan angles and relative azimuth angles changed significantly. The illumination and viewing geometry changes affect the AVHRR visible channel reflectances because of the anisotropic reflection and asymmetrical scattering characteristics of snow and clouds, which must be taken into account for surface albedo retrieval.

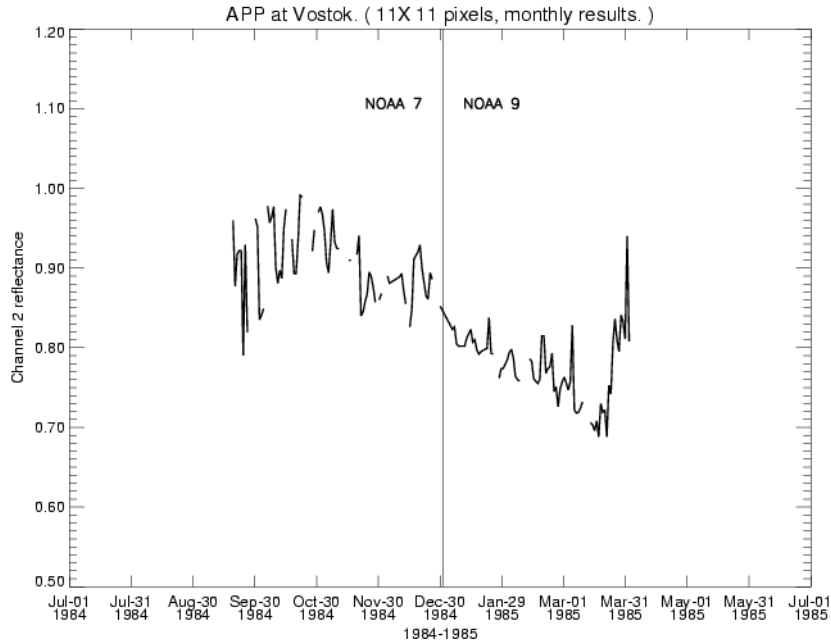


**Figure 10: Time series of the AVHRR channel 2 reflectance averaged over a 275 x 275 km<sup>2</sup> area around Vostok, Antarctica from July 1, 1984 to July 1, 1985 at a local solar time of 1400, covering the transition of NOAA-7 to NOAA-9.**

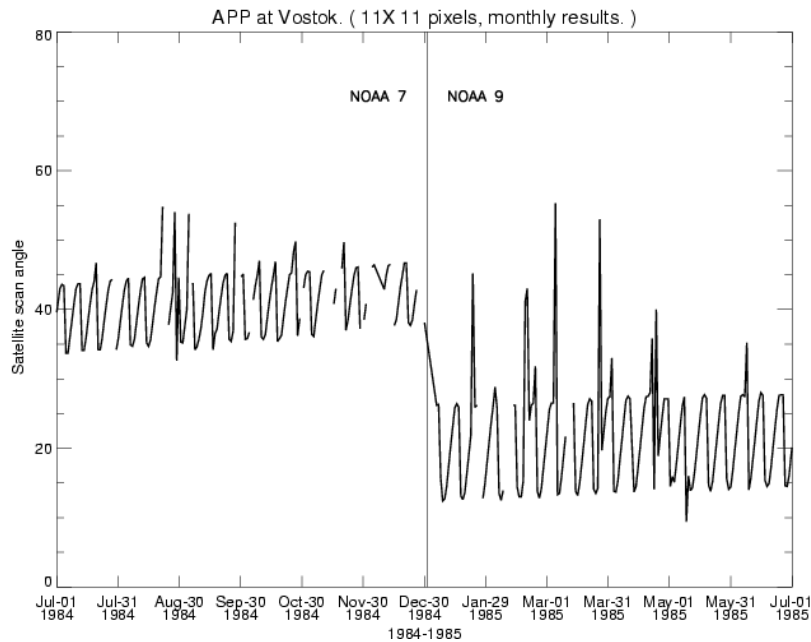


**Figure 11: Time series of the AVHRR scan angle averaged over a 275 x 275 km<sup>2</sup> area around Vostok, Antarctica from July 1, 1984 to July 1, 1985 at a local solar time of 1400, covering the transition of NOAA-7 to NOAA-9.**

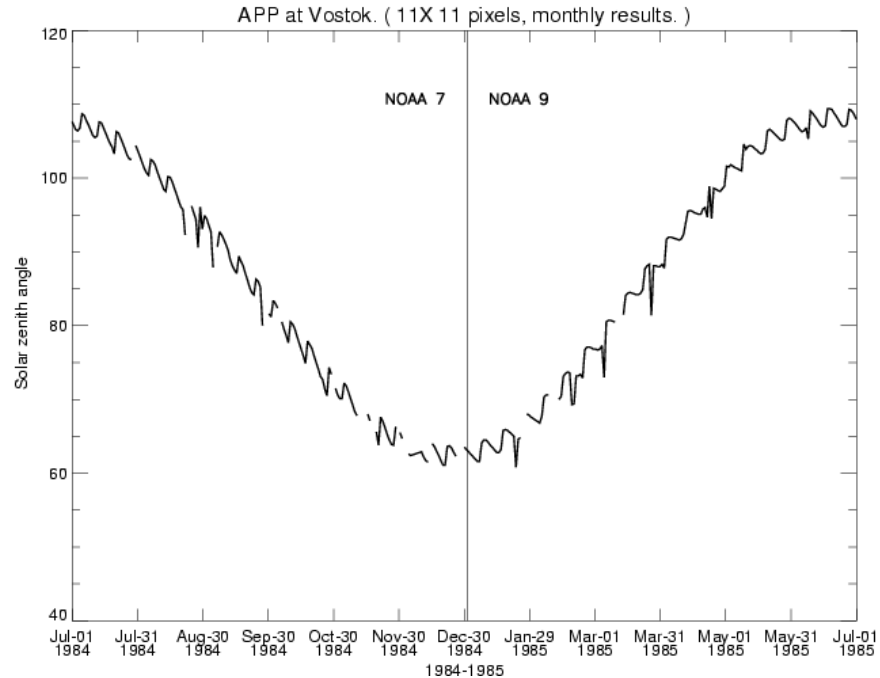


**Figure 12: Time series of the solar zenith angles averaged over a 275 x 275 km<sup>2</sup> area around Vostok, Antarctica from July 1, 1984 to July 1, 1985 at local solar time of 1400, covering the transition from NOAA-7 to NOAA-9.**

The differences of APP v1.0 and v2.0 are manifested in the differences of the visible channel reflectance. The mean visible channel reflectance difference on some days can be as high as around 3%, with higher differences on individual grids; the infrared channel brightness temperature differences are negligible. Figure 13 show an example of the differences of reflectance differences of Channel 2, and brightness temperature differences of Channel 4 on July 15, 2016.

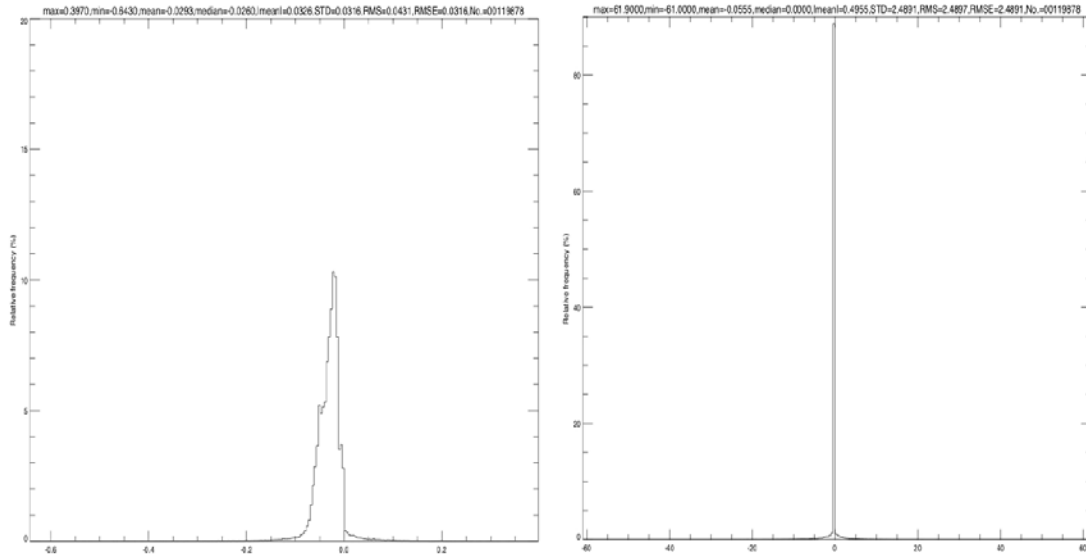


**Figure 13: Histogram of Channel 2 reflectance differences (left), and Channel 4 brightness temperature differences at local solar time of 1400 on July 15, 2016.**

## 6.2 Sensor Performance

Degradation of the AVHRR visible channel is addressed explicitly in the reflectance channel calibration method employed here. Thermal channels have on-board calibration so sensor degradation is not an issue.

## 7. Future Enhancements

### 7.1 Enhancement 1

Currently, the quality assessment and diagnostics are done by checking the quality of the Advanced AVHRR Polar Pathfinder dataset (APP-x), which derives higher-level geophysical parameters from the APP product. Quality assessment and diagnostics specific to APP are being designed and will be implemented in the future. The quality assessment approach includes automatic daily composite display and monitoring of time series of variables derived in APP-x.

## 8. References

- Cavaliere, D. J., P. Gloersen, and H. Zwally. Edited by J. Maslanik and J. Stroeve, 1999, Near-Real-Time DMSP SSMIS Daily Polar Gridded Brightness Temperatures. Boulder, Colorado USA: NASA National Snow and Ice Data Center Distributed Active Archive Center. <http://dx.doi.org/10.5067/AKQDND71ZDLF>.
- Foster, J.M., and A. Heidinger, 2013, PATMOS-x: Results from a diurnally corrected 30-year satellite cloud climatology. *Journal of Climate*, Volume 28, Issue 2, pp. 414-425.
- Goodison, B. E. ,1989, Determination of Areal Snow Water Equivalent on the Canadian Prairies Using Passive Microwave Satellite Data. *IGARSS '89 Proceedings* 3:1243-1246.
- Heidinger, A.K., W.C. Straka III, C.C. Molling, J.T. Sullivan, and X. Wu, 2010, Deriving an inter-sensor consistent calibration for the AVHRR solar reflectance data record. *International Journal of Remote Sensing*, Volume 31, Issue 24, pp. 6493-6517.
- Heidinger, A. K. et al., 2002, Using Moderate Resolution Imaging Spectrometer (MODIS) to calibrate Advanced Very High Resolution Radiometer reflectance channels. *Journal of Geophysical Research*. Vol. 107. doi: 10.1029/2001JD002035.
- Key, J. R., and J. M. Intrieri, 2000, Cloud particle phase determination with the AVHRR, *J. Appl. Meteorol.*, 39, 1797– 1804.
- Key, J. R., X. Wang, J. C. Stoeve, and C. Fowler, 2001, Estimating the cloudy-sky albedo of sea ice and snow from space, *J. Geophys. Res.*, 106, 12,489– 12,497, doi:10.1029/2001JD900069.
- Key, J., P. Yang, B. Baum, and S. Nasiri, 2002, Parameterization of shortwave ice cloud optical properties for various particle habits, *J. Geophys. Res.*, 107(D13), 4181, doi:10.1029/2001JD000742.
- Kidwell, Katherine B., comp. and ed., 1995, NOAA Polar Orbiter Data (TIROS-N, NOAA-6, NOAA-7, NOAA-8, NOAA-9, NOAA-10, NOAA-11, NOAA-12, and NOAA-14) Users Guide: Washington, D.C., NOAA/NESDIS, <http://www.ncdc.noaa.gov/oa/pod-guide/ncdc/docs/podug/>.
- Kidwell, Katherine B., comp. and ed., 2009, NOAA KLM User's Guide with NOAA-N, -P Supplement (February 2009 Revisions), <http://www.ncdc.noaa.gov/oa/pod-guide/ncdc/docs/klm/index.htm>.
- Liu, Y., J. R. Key, and X. Wang, 2008, The influence of changes in cloud cover on recent surface temperature trends in the Arctic, *J. Clim.*, 21, 705– 715, doi:10.1175/2007JCLI1681.1.
- Molling, C.C., A.K. Heidinger, W.C. Straka III, and X. Wu, 2010, Calibrations for AVHRR channels 1 and 2: review and path towards consensus. *International Journal of Remote Sensing*, 31:6519 - 6540.

- Nolin, A. W., R. Armstrong, and J. Maslanik. 1998. Near-Real-Time SSM/I-SSMIS EASE Grid Daily Global Ice Concentration and Snow Extent. Version 4. Boulder, Colorado USA: NASA DAAC at the National Snow and Ice Data Center.
- Robel, J., Ed., 2009, NOAA KLM User's Guide with NOAA-N, -N0 Supplement. Available online at: <http://www.ncdc.noaa.gov/oa/pod-guide/ncdc/docs/intro.htm>
- Sullivan, J. and Jelenak, A., 2007, Correcting Geo-Location Interpolation Errors in Nesdis-Produced AVHRR 1b Data near the Poles. *International Journal of Remote Sensing*, 28(16), 3721-3728. [10.1080/01431160701313818]
- Trischenko, A. P., G. Fedosejevs, Z. Li, and J. Cihlar, 2002, Trends and uncertainties in thermal calibration of AVHRR radiometers onboard NOAA-9 to -16, *J. Geophys. Res.*, 107(D24), 4778, doi:10.1029/2002JD002353.
- Wang, X. J., and J. R. Key, 2003, Recent trends in arctic surface, cloud, and radiation properties from space, *Science*, 299, 1725 – 1728, doi:10.1126/science.1078065.
- Wang, X. J., and J. R. Key, 2005a, Arctic surface, cloud, and radiation properties based on the AVHRR Polar Pathfinder dataset. Part I: Spatial and temporal characteristics, *J. Clim.*, 18, 2558 – 2574, doi:10.1175/JCLI3438.1.
- Wang, X. J., and J. R. Key, 2005b, Arctic surface, cloud, and radiation properties based on the AVHRR Polar Pathfinder dataset. Part II: Recent trends, *J. Clim.*, 18, 2575– 2593, doi:10.1175/JCLI3439.1.

## Appendix A. Acronyms and Abbreviations

Acronym or Abbreviation	Meaning
APP	AVHRR Polar Pathfinder
APP-x	eXtended AVHRR Polar Pathfinder (APP)
AVHRR	Advanced Very High Resolution Radiometer
C-ATBD	Climate Algorithm Theoretical Basis Document
CDR	Climate Data Record
CIMSS	Cooperative Institute for Meteorological Satellite Studies, University of Wisconsin-Madison
EASE	Equal-Area Scalable Earth
EUMETSAT	European Organization for the Exploitation of Meteorological Satellites
ESA	European Space Agency
IDL	Interactive Data Language
MODIS	Moderate-resolution Imaging Spectroradiometer
NASA	National Aeronautics and Space Administration
NCDC	National Climatic Data Center
NCEP	National Centers for Environmental Prediction
NESDIS	NOAA's Satellite and Information Service
NOAA	National Oceanic and Atmospheric Administration
NSIDC	National Snow and Ice Data Center
SSEC	Space Science and Engineering Center, University of Wisconsin-Madison
STAR	The Center for Satellite Applications and Research
UW-Madison	University of Wisconsin-Madison